Available online at www.sciencedirect.com

ScienceDirect

Procedia Engineering 109 (2015) 364 – 371

Procedia Engineering

www.elsevier.com/locate/procedia

XXIII Italian Group of Fracture Meeting, IGFXXIII

A FE-Meshless multiscale approach for masonry materials

Antonino Spada*[a], Giuseppe Giambanco[a], Emma La Malfa Ribolla[a]

[a]*Department of Civil, Environmental, Aerospace Engineering and Materials (DICAM)*
University of Palermo, Viale delle Scienze Ed. 8, 90128 Palermo, Italy

Abstract

A FE-Meshless multiscale computational strategy for the analysis of running bond masonry is presented. The Meshless Method (MM) is adopted to solve the boundary value problem (BVP) at the mesoscopic level. The representative unit cell is composed by the aggregate and the surrounding joints, the former assumed to behave elastically while the latter are simulated as non-associated elastic-plastic zero-thickness interfaces with a softening response. Macroscopic localization of plastic bands is obtained performing a spectral analysis of the tangent stiffness matrix. Localized plastic bands are embedded into the quadrature points area of the macroscopic finite elements.

Peer-review under responsibility of the Gruppo Italiano Frattura (IGF)

Keywords: Computational Homogenization; Meshless; Masonry; Localization; Interfaces.

1. Introduction

In heterogeneous materials, the most relevant kinematic and mechanical phenomena take place at a scale which is small if compared to the dimensions of the structure. On the other side, the structure is governed by its global geometrical and morphological configuration. Joints often represent the weakness zones of the structure.
In literature two different scales of interest are distinguished. In the *mesoscopic* approach the constituents and their interfaces are considered individually. Most of the efforts in this research area are concentrated on the formulation of advanced interface constitutive laws capable to describe the damage evolution and the onset of irreversible strains for different mechanical problems or materials ([1]-[9]). In the *macroscopic* approach the structure is constituted by a fictitious homogeneous and continuous material. In this approach simplified constitutive models are formulated in a phenomenological manner, intentionally neglecting the actual material composition but smearing the effects of the heterogeneities presence by apposite mechanical assumptions (Fuschi *et al.* [10]). To this approach the multiscale techniques belong. These techniques couple different scales of interest by means of apposite transition laws capable to exchange information between different consecutive scales.
Multiscale modeling of heterogeneous materials is developed in the framework of homogenization methods when in

* Corresponding author. Tel.: +39-091-238-96709 ; fax: +39-091-427121.
E-mail address: antonino.spada@unipa.it

Peer-review under responsibility of the Gruppo Italiano Frattura (IGF)
doi:10.1016/j.proeng.2015.06.244

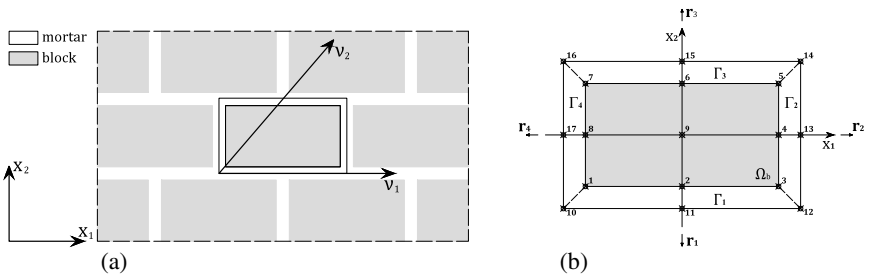

Fig. 1. (a) Unit cell extracted from running bond masonry. (b) Meshless discretization.

the structure separated scales can be clearly identified. The Computational Homogenization (CH) strategy is the most diffused among those present in literature ([11]). A macroscopic strain or stress is used to apply kinematic or static boundary conditions to the init cell (UC) (*macro-meso scale transition*). The equilibrium of the UC is obtained by solving a boundary value problem (BVP) at the mesoscale. Lastly, the macro-strain or macro-stresses are assumed to be the average on the UC of the corresponding meso-strain or meso-stresses (*meso-macro scale transition*).
In the first-order CH methods, Cauchy models are used at all scales ([12], [13]). These methods are based on the *Principle of Separation of Scales* ([14]). The finite element method is usually applied at both scales. Giambanco *et al.* [15] used instead the Meshless Method ([16]) to solve the BVP at the mesoscale. In the second-order CH methods, Cosserat or higher order continua are considered at the macroscopic level ([17], [18]).
The eventual concentration of inelastic deformations at the UC interfaces involves the possibility to localize inelastic deformations even at the macroscale, that are usually introduced in a smeared sense in the FE mesh. Rice [19] stated that the process of localization of deformation can be viewed as an instability (discontinuity bifurcation) that can be predicted in terms of constitutive relations of the material. Once a band is localized, it is inserted into the finite element macroscopic mesh as an embedded discontinuity. Belytschko *et al.* [20] modify the quadrature scheme introducing an averaging procedure based on the fraction of the localized area with respect to the total one.
In this paper we present an extension of the conventional first-order CH method. The formulation of the UC BVP is developed in the framework of Meshless Methods instead of the classic mesh-based methods. Mesh-based methods are time-consuming and dependent on the mesh refinement required to correctly catch the inelastic phenomena at the mesoscale. The theory of discontinuous bifurcation is applied to localize plastic deformations at the macroscale. The localization of a plastic band is obtained performing a spectral analysis of the macroscopic tangent stiffness matrix, that is evaluated on the base of the solution of UC BVP. The localized band is inserted at the macroscopic FE mesh following the smeared approach. The averaging procedure proposed by Belytschko *et al.* [20] is applied.
A numerical application on a masonry wall is employed to assess the goodness of the proposed model.

2. Basics of the CH scheme and Meshless solution of the UC at the mesoscale.

Let us consider a structure constituted by a heterogeneous material at the mesoscale. The continuous structure is discretized in a finite number of sub-domains or elements. As shown in Figure 1(a), given the geometrical configuration of the masonry structure, a single finite element can include different blocks which a UC, constituted by a single block surrounded by half of the joint thickness can be extracted from.
The weak form of equilibrium written for the UC provides the following conditions:

$$\bar{\mathbf{u}}_m = \mathbf{D}_m \, \varepsilon_{\mathbf{M}} \tag{1}$$

$$\sigma_{\mathbf{M}} = \frac{1}{|\Omega_{UC}|} \int_{\Gamma_{UC}} \mathbf{D}_m^T \mathbf{r} \mathrm{d}\Gamma. \tag{2}$$

where $\mathbf{u_m}$ is the displacement of a point at the mesoscale, $\varepsilon_\mathbf{M}$ and $\sigma_\mathbf{M}$ the macroscopic strain and stress fields, Ω_{UC} the area of the UC, having boundary Γ_{UC}.

$$\mathbf{D}_m = \begin{bmatrix} x_1 & 0 & x_2/2 \\ 0 & x_2 & x_1/2 \end{bmatrix}. \tag{3}$$

Equations (1-2) are the macro-meso and meso-macro transition conditions adopted for the multiscale problem. Equation 1 consists in the evaluation of the linear boundary conditions to be applied to the UC, while equation 2 is based on the Hill-Mandel principle.
The material of the block is considered indefinitely elastic, while the joints are simulated as zero thickness interfaces (ZTI). The interface constitutive laws are developed in the framework of elastoplasticity for non standard materials. Making use of the meshless approximation procedure illustrated by Giambanco *et al.* [15] and with reference to Figure 1(b), the following governing equations are obtained:

$$\begin{bmatrix} \mathbf{K} & -\mathbf{G} \\ \mathbf{G}^T & \mathbf{0} \end{bmatrix} \begin{bmatrix} \mathbf{U}_m \\ \mathbf{R} \end{bmatrix} = \begin{bmatrix} \mathbf{F}_p \\ \bar{\mathbf{U}}_m \end{bmatrix} \tag{4}$$

where

$$\mathbf{K} = \int_{\mathbf{\Omega_b}} \mathbf{S_b^T \Phi_b^T C^T E_b C \Phi_b S_b} \mathrm{d}\Omega + \sum_{\mathbf{k=1}}^{\mathbf{4}} \int_{\mathbf{\Gamma_k}} \mathbf{(\Phi_i S_i - \Phi_b S_b)^T T_i^T E_i \, T_i \, (\Phi_i S_i - \Phi_b S_b)} \, \mathbf{d\Gamma} \tag{5}$$

$$\mathbf{G} = \sum_{k=1}^{4} \int_{\Gamma_k} \mathbf{S}_i^T \mathbf{\Phi_i^T \Psi_i \bar{S}}_i d\Gamma \tag{6}$$

$$\mathbf{F}_p = \sum_{k=1}^{4} \int_{\Gamma_k} (\mathbf{\Phi_i S}_i - \mathbf{\Phi_b S}_b)^T \, \mathbf{T}_i^T \mathbf{E}_i \, [\mathbf{u}_m]^p \, d\Gamma \tag{7}$$

$$\bar{\mathbf{U}}_m = \sum_{k=1}^{4} \int_{\Gamma_k} \bar{\mathbf{S}}_i^T \mathbf{\Phi}_i^T \bar{\mathbf{u}}_m d\Gamma. \tag{8}$$

$\mathbf{E}_b$ and $\mathbf{E}_i$ are the elastic stiffness matrices of block and mortar respectively. S_b, S_i, and $\bar{S}_i$ are selectivity matrices. $\mathbf{\Phi}_b$ and $\mathbf{\Phi}_i$ are meshless form function matrices. $\mathbf{T}$ is a rotation matrix while $[\mathbf{u}_m]^p$ the plastic displacement discontinuity at the interface. In order to evaluate the integrals (5)÷(8), the Gauss quadrature rule is adopted with nine sample points in the block domain and three sample points for each interface.
Calculating the inverse of coefficient matrix the solution can be given by as:

$$\mathbf{U}_m = \mathbf{B}_{11} \, \mathbf{F}_p + \mathbf{B}_{12} \, \bar{\mathbf{U}}_m \tag{9}$$

$$\mathbf{R} = \mathbf{B}_{21} \, \mathbf{F}_p + \mathbf{B}_{22} \, \bar{\mathbf{U}}_m. \tag{10}$$

The elastic domain for the interfaces is defined by a Coulomb bilinear limit surface and a tension cut-off:

$$\Phi^{p1}(\sigma_{\mathbf{mi}}, \chi^p) = |\tau_{\mathbf{mi}}| + \sigma_{mi} \tan\phi - c_0(1 - \chi^p), \tag{11}$$

$$\Phi^{p2}(\sigma_{\mathbf{mi}}, \chi^p) = \sigma_{mi} - \sigma_0(1 - \chi^p), \tag{12}$$

where $\tau_{\mathbf{mi}}$ and σ_{mi} are the tangential stress vector and the normal stress component of the contact stresses, ϕ is the friction angle, c_0 and σ_0 the cohesion and tensile strength of the virgin interfaces. χ^p is a static variable which is associated to the internal variable ξ^p which regulates the isotropic hardening-softening interface behavior:

$$\chi^p = h^p \xi^p, \tag{13}$$

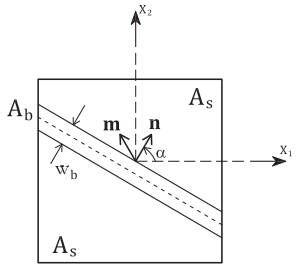

Fig. 2. Body with a plastic band inside.

with h^p the hardening-softening parameter.
The inelastic displacement discontinuities develop according to non-associative flow rules:

$$[\dot{\mathbf{u}}_m]^p = \dot{\lambda}^{p1}\frac{\partial G^p}{\partial \sigma_{\mathbf{mi}}} + \dot{\lambda}^{p2}\frac{\partial \Phi^{p2}}{\partial \sigma_{\mathbf{mi}}}, \quad \dot{\xi}^p = -\dot{\lambda}^{p1}\frac{\partial \Phi^{p1}}{\partial \chi^p} - \dot{\lambda}^{p2}\frac{\partial \Phi^{p2}}{\partial \chi^p}, \tag{14}$$

where $\dot{\lambda}^{p1}$, $\dot{\lambda}^{p2}$ are the plastic multipliers which satisfy the common complementarity conditions. The plastic potential related to the limit condition (11) is expressed by the following function:

$$G^p(\sigma^{\mathbf{c}}, \chi^p) = |\tau_{\mathbf{mi}}| + \sigma_{mi}(1-\chi^p)\tan\delta - r, \tag{15}$$

with $\delta \in [0, \phi]$ dilatancy angle and r an arbitrary material constant.

3. Plastic bands localization and insertion on macroscale finite element

Let us consider an element with a localized region (plastic band, b) and a non-localized sound region s (Figure 2). The plastic band is separated from the remaining part by weak discontinuity surfaces.

Equilibrium and compatibility conditions across a discontinuity line have to be respected. Including also the constitutive relations for the two regions the following equation is obtained ([19]):

$$\left(\mathbf{C}_n^T \mathbf{E}_b^t \mathbf{C}_n\right)\dot{g}\,\mathbf{m} = \mathbf{C}_n^T\left(\mathbf{E}_b^t - \mathbf{E}_s^t\right)\dot{\varepsilon}_{\mathbf{s}} \tag{16}$$

where $\mathbf{C}_n$ is the compatibility matrix written for a point on a surface whose normal unit vector is $\mathbf{n}$, $\mathbf{E}_b^t$ and $\mathbf{E}_s^t$ the stiffness tangent matrices on the plastic and sound regions respectively, $\dot{\varepsilon}_s$ the strain rate in the sound region. $\dot{g}$ is a measure of the strain rate jump. $\mathbf{m}$ is a unit vector called polarization vector.
When no plastic bands are present, $\mathbf{E}_b^t = \mathbf{E}_s^t = \mathbf{E}^t$. In this case the condition of incipient localization is given by

$$\det \mathbf{L} = 0. \tag{17}$$

where $\mathbf{L} = \mathbf{C}_n^T \mathbf{E}^t \mathbf{C}_n$ is called localization or *acoustic tensor*.
Once the plastic band is present, the two materials exhibit different constitutive behaviors, and the tangent stiffness matrices are no longer identical. This particular case is called discontinuous bifurcation, and condition (16) has to be respected. In this case

$$\mathbf{E}_b^t = \mathbf{E}_M^{et} + \mathbf{E}_M^{pt} \tag{18}$$

$$\mathbf{E}_s^t = \mathbf{E}_M^{et} \tag{19}$$

where

$$\mathbf{E}_M^{et} = \frac{1}{\Omega_{UC}}\mathbf{Q}\,\mathbf{B}_{22}\mathbf{Q}^T \tag{20}$$

$$\mathbf{E}_M^{pt} = \frac{1}{\Omega_{UC}} \mathbf{Q}\,\mathbf{B}_{21}\,(\mathbf{I} - \mathbf{P}\,\mathbf{B}_{11})^{-1}\mathbf{P}\,\mathbf{B}_{12}\,\mathbf{Q}^T \tag{21}$$

with

$$\mathbf{Q} = \sum_{k=1}^{4} \int_{\Gamma_k} \mathbf{D}_m^T \mathbf{\Phi}_\mathbf{i} \bar{\mathbf{S}}_i d\Gamma \tag{22}$$

$$\mathbf{P} = \sum_{k=1}^{4} \int_{\Gamma_k} (\mathbf{\Phi}_\mathbf{i}\mathbf{S}_i - \mathbf{\Phi}_\mathbf{b}\mathbf{S}_b)^T \mathbf{T}_i^T \mathbf{E}_i \frac{\partial [\mathbf{u}_m]^p}{\partial [\mathbf{u}_m]} \mathbf{T}_i\,(\mathbf{\Phi}_\mathbf{i}\mathbf{S}_i - \mathbf{\Phi}_\mathbf{b}\mathbf{S}_b)\,d\Gamma. \tag{23}$$

An explanation on how equations (20), (21), and (23) are obtained is given in Giambanco *et al.* [15].
In the case of a discontinuous bifurcation, it has been proved that ([13], [20]):

$$\det \mathbf{L} \leq 0; \quad \lambda_{min} \leq 0. \tag{24}$$

The unit vectors **m** and **n** define the nature of the discontinuity. When the **n** direction is localized, a plastic band is included in the area of the generic macroscopic Gauss point. The integration over the entire finite element is done on the base of the modified quadrature scheme suggested by Belytschko *et al.* [20]. The modified quadrature scheme consists into separate the generic function $F(\xi)$ to be integrated in two values, one ($F_b(\xi)$) correspondent to the behavior of the material in the band, one ($F_s(\xi)$) correspondent to the behavior in the elastic portion, each one weighted for the correspondent area fraction f_b or f_s.
The stress rate and the tangential stiffness matrix at the macroscopic level are obtained as:

$$\dot{\sigma}_\mathbf{M} = f_b\,\dot{\sigma}_\mathbf{b} + f_s\,\dot{\sigma}_\mathbf{s}, \tag{25}$$

$$\mathbf{E}_M^t = f_b\,\mathbf{E}_b^t + f_s\,\mathbf{E}_s^t. \tag{26}$$

An important point is how to evaluate the band area. In author's knowledge, this can be done following a phenomenological procedure, acquiring information about the failure pattern of a running bond masonry subjected to a generic boundary load. With reference to the work of Dhanasekar *et al.* [21], three particular cases are selected, namely considering the uniaxial tension acting with an angle of 0^o, β, or 90^o with respect to the bed joints. A correspondence between the localization α angle and the band width w_b is defined. For intermediate values of α a linear variation of w_b is considered. The band length is assumed equal to the length of the middle line of the band.

4. Numerical procedure

Three nested iterative procedures are employed: one for the macroscopic classical finite element solution, one for the localization at the quadrature point, one for the mesoscopic BVP solution.
At $t = 0$, the elastic stiffness matrix for the homogenized material is evaluated. At the generic time step $[t_n, t_{n+1}] \subset [0, T]$ the increment of the macroscopic strain at a single Gauss point of the homogenized structure is obtained. Two different situations can be found at the macroscopic Gauss point. The first case is that one of a Gauss point without localized plastic band. The second case is when a plastic band is present. In the first case the entire macroscopic strain increment is imposed to the UC and the resultant stress increment is attributed to the macroscopic Gauss point. In the second case the macroscopic strain increment is separated in a contribute afferent to the plastic band and a contribute afferent to the sound region. The strain rates are evaluated solving the following system:

$$\begin{cases} \mathbf{C}_n^T \mathbf{E}_b^t\,\dot{\varepsilon}_b = \mathbf{C}_n^T \mathbf{E}_s^t\,\dot{\varepsilon}_s \\ \dot{\varepsilon}_M = f_b\,\dot{\varepsilon}_b + f_s\,\dot{\varepsilon}_s \end{cases}. \tag{27}$$

The stress increments are therefore calculated for the two regions on the base of their own strain increments. In particular, the $\dot{\sigma}_\mathbf{b}$ stress rate is evaluated solving the BVP with imposed $\dot{\varepsilon}_b$ strain rate. The BVP is solved through an iterative loop. **K** matrix and $\delta\mathbf{F}_p$ are updated at each iteration untill the convergence condition

$$\left|\Delta\mathbf{U}_m^{p,j} - \Delta\mathbf{U}_m^{p,j-1}\right| < tol \tag{28}$$

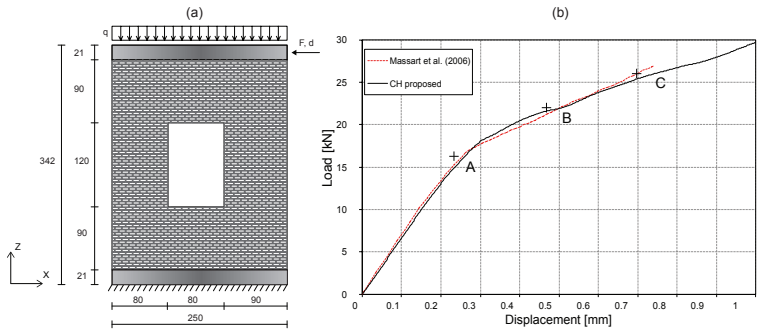

Fig. 3. Masonry wall of Massart *et al.* [13]. (a) Geometry; (b) Load-displacement curves.

is reached. The $\dot{\sigma}_s$ stress rate is obtained assuming the sound region to unload elastically. At the same time, the macroscopic tangent stiffness matrix in the plastic band is updated. Material tangent matrix is used to localize the new macroscopic plastic band orientation through a spectral analysis of the associated acoustic tensors. When a new plastic band is formed, or simply it changed orientation with respect to the previous iteration, the values of the strain increment on the non-localized and localized regions have to be updated and quantities reevaluated. At the end of the loop, the final stress increment and global tangent stiffness matrix at the macroscopic quadrature point are calculated. The finite element tangential stiffness matrix and internal force vector are finally assessed according to the modified quadrature scheme proposed.
The nonlinearity of the problem may lead to a possible lack of convergence at the macroscopic level for the n^{th} step of the Newton-Raphson iterative procedure. In this case the numeric procedure needs a further iteration, reevaluating the macroscopic strains for each FE Gauss point and associating them to the stresses coming from the analysis at the mesoscale. When even the convergence of the finite element analysis at the macroscale level is reached, the program skips to the next load step.

5. Numerical application

The FE·Meshless multiscale computational strategy presented is applied to simulate the masonry shear wall test proposed by Massart *et al.* [13].
The geometry of the wall is shown in Figure 3. Each brick is 90 mm long, 30 mm high, 100 mm wide, with 10 mm thick mortar joints. The top and bottom boundaries of the wall are considered clamped. The load is applied in two phases. In a first phase, the wall is compressed by a uniformly distributed load obtained imposing a uniform vertical displacement on the top boundary of the wall. In a second phase, maintaining constant the distributed compressive load, a monotonically increasing horizontal shear load is applied.
Like a classic FE^2 multiscale procedure, Massart *et al.* [13] adopted FE meshes at the two scales. Periodic boundary conditions were imposed on the UC. The UC coincided with a block and surrounding mortar joints. At the macroscale, 48 elements with a biquadratic displacement interpolation and four integration points were used. The lower and upper bands of elements had an elastic behavior, in order to simulate the presence of two steel beams restraining the wall. A resultant compressive vertical load of 37.5 KN was applied.
In our work the same numerical example is reproduced. As such, an identical macroscopic FE configuration has been considered.

Table 1. Mechanical parameters adopted in the analysis.

E_b (MPa)	ν_b	E_s (MPa)	ν_s	c_0 (MPa)	σ_0 (MPa)	h_p $(MPa)^{-1}$	φ $(^o)$	δ $(^o)$
16700	0.15	3900	0.20	0.18	0.13	40	37	$1/2\,\varphi$

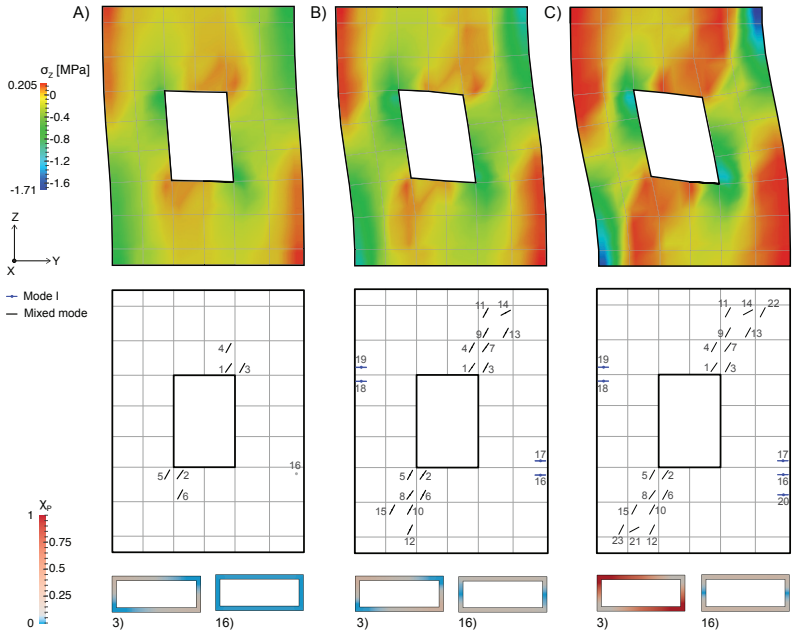

Fig. 4. Stress profiles on deformed shape and results of localization.

At the mesoscale level, a mesfree UC composed by a brick with dimensions 90 x 30 mm^2 surrounded by half thickness of mortar joint is considered. The mechanical parameters adopted are reported in Table 1.

The results in terms of load-displacement curves are shown in Figure 3. The proposed procedure generates a curve that well agrees with the numerical one produced by the model of Massart *et al.* [13]. In particular, after an almost identical elastic behaviour, approximately the same nonlinear branch is captured. The numerical curve finally continues with no significant changes in its slope. This is the result of the lack of a cup mode for compressive failure.

In Figure 4 the results in terms of vertical stresses and the correspondent localization patterns at the three points A, B, and C indicated in the load-displacement curve are reported. The macroscopic stress is plot on the deformed shape of the wall. Displacements are magnified by a factor of 500. Tensile stresses appear first at the lower left and top right corners of the opening and at the lower right and top left corners of the wall (point A). In the same regions a more intense stress profile is visible at point B and even more at point C.

The evolution of embedded localization bands at Gauss points is also shown in Figure 4 for the same time steps. Numbers indicate the progressive order of appearance of localized bands in the elements. Bands are also distinguished between mixed mode bands and splitting tensile mode I bands. At the beginning of the nonlinear branch few bands are visible (point A). The first failure mechanism is in fact taking place, consisting in two diagonal cracks starting from the corners of the opening and evolving towards the corners of the wall. In the last line of Figure 4 the evolution of plasticity at the mesoscale is reported for the Gauss points 3 and 16. The value of χ^p variable is depicted in color at the mortar joints, since the brick is maintained elastic. A typical staircase evolution of plasticity characterizes point 3, respecting the mixed mode nature of the band. Point 16 is instead still sound, without any localization band.

At point B the second failure mechanism initiates its process. It consists in the developing of horizontal bands at the two sides of the wall, in an opposite position with respect to the existing bands. While all the inclined embedded bands evolve in a mixed mode, due to the contemporary action of vertical and shear strains, these new bands evolve in mode I, as it is clearly showed by the mesoscopic localization map.

At point C the diagonal cracks are completed. Embedded bands are present in almost all the elements included between the top right corner of the opening and the top right corner of the wall and from the lower left corner of the opening to that one of the wall. Other horizontal cracks in mode I are present close to the previous ones. The identifi-

cation of the critical zones is also supported by the deformed shape of the mesh. The finite elements where localization takes place are strongly distorted, because subjected to a great amount of strain concentrated inside the element.

6. Conclusions

The paper presents a computational homogenization method implemented to model structures constituted by running bond masonry. The computational homogenization strategy proposed is able to reproduce the linear and nonlinear mechanical response of the structure at the macro-level on the base of the results of the boundary value problem defined for the mesoscopic unit cell. The equilibrium problem of the structure is discretized making use of the finite element method and the unit cell is solved by means of a meshless model. A novelty which characterizes the proposed numerical strategy is the adoption of the meshless method to analyze the unit cell. The paper also introduces the concept of zero-thickness interface elements in a multiscale procedure, to simulate the inelastic phenomena occurring at the mesoscale. The classical theory of discontinuous bifurcation is applied to identify localization bands. The localized band is inserted in a Gauss quadrature area in a smeared sense, averaging the kinematical and mechanical quantities over the integration domain. The defined computational homogenization strategy has been validated through a numerical examples. The example shows the capability of the model to catch the same results of the enhanced multiscale model of Massart *et al.* [13].

References

[1] G. Giambanco, S. Rizzo, R. Spallino, Numerical analysis of masonry structures via interface models, Comput. Methods Appl. Mech. Eng. 190 (49) (2001) 6493-6511.
[2] P.B. Lourenço, J.G. Rots, Multisurface interface model for analysis of masonry structures, J. Eng. Mech. (ASCE) 123 (7) (1997) 660-668.
[3] G. Giambanco, G. Fileccia Scimemi, Mixed mode failure analysis of bonded joints with rate-dependent interface models, Int. J. Numer. Methods Eng. 67 (8) (2006) 1160-1192.
[4] A. Spada, G. Giambanco, P. Rizzo, Damage and plasticity at the interfaces in composite materials and structures, Comput. Methods Appl. Mech. Engrg. 198 (49) (2009) 3884-3901.
[5] A. Spada, G. Giambanco, P. Rizzo, Elastoplastic Damaging Model for Adhesive Anchor Systems. I: Theoretical Formulation and Numerical Implementation, J. Eng. Mech. 137 (2011) 854-861.
[6] E. Sacco, F. Lebon, A damage-friction interface model derived from micromechanical approach, Int. J. Solids and Struct. 49 (26) (2012) 3666-3680.
[7] G. Alfano, M.A. Crisfield, Finite element interface models for the delamination analysis of laminated composite: mechanical and computational issues, Int. J. Numer. Meth. Eng. 50 (7) (2001) 1701-1736.
[8] G. Giambanco, G. Fileccia Scimemi, A. Spada, The interphase finite element, Computational Mechanics 50 (3) (2012) 353-366.
[9] G. Fileccia Scimemi, G. Giambanco, A. Spada, The interphase model applied to the analysis of masonry structures, Comput. Methods Appl. Mech. Engrg. 279 (2014) 66-85.
[10] P. Fuschi, G. Giambanco, S. Rizzo, Nonlinear finite element analysis of no-tension masonry structures, Meccanica 30 (3) (1995) 233-249.
[11] V.P. Nguyen, M. Stroeven, L.J. Sluys, Multiscale continuous and discontinuous modeling of heterogeneous materials: A review on recent developments, J. Multiscale Model. 3 (04) (2011) 229-270.
[12] F. Feyel, J.L. Chaboche, FE^2 multiscale approach for modelling the elastoviscoplastic behavior of long fibre SiC/Ti composite materials, Comput. Methods Appl. Mech. Eng. 183 (3) (2000) 309-330.
[13] T.J. Massart, R.H.J. Peerlings, M.G.D. Geers, An enhanced multi-scale approach for masonry wall computations with localization of damage, Int. J. Numer. Meth. Engng. 69 (2007) 1022-1059.
[14] M.G.D. Geers, V.G. Kouznetsova, W.A.M. Brekelmans, Multi-scale computational homogenization: Trends and challenges, J. Comput. Appl. Math. 234 (7) (2010) 2175-2182.
[15] G. Giambanco, E. La Malfa Ribolla, A. Spada, CH of masonry materials via meshless meso-modeling, Frattura ed Integrita′ Strutturale 29 (2014) 150-165.
[16] S.N. Atluri, S. Shen, The meshless method, Tech. Sci. Press, Forsyth, 2002.
[17] D. Addessi, E. Sacco, A. Paolone, Cosserat model for periodic masonry deduced by nonlinear homogenization, Eur. J. Mech. A Solids. 29 (4) (2010) 724-737.
[18] D. Addessi, E. Sacco, A multi-scale enriched model for the analysis of masonry panels, Int. J. Solids and Struct. 49 (6) (2012) 865-880.
[19] J.R. Rice, The localization of plastic deformation, Theoretical and Applied Mechanics (Proceedings of the 14th International Congress on Theoretical and Applied Mechanics, Delft, 1976), 1 (1976) 207-220.
[20] T. Belytschko, J. Fish, B.E. Engelmann, A finite element with embedded localization zones, Comput. Methods Appl. Mech. Engrg. 70 (1988) 59-89.
[21] M. Dhanasekar, A.W. Page, P.W. Kleeman, The failure of brick masonry under biaxial stresses, Proc. Instn Civ. Engrs. 79 (1985) 295-313.